Total Variation Algorithms for PAT Image Reconstruction

Mary Josy John and Imad Barhumi
College of Engineering, United Arab Emirates University, Al Ain, UAE
E-mail: 201990198@uaeu.ac.ae, imad.barhumi@uaeu.ac.ae

***Abstract*—Medical imaging is an essential part of disease diagnosis, which makes use of technologies such as X-ray, Magnetic Resonance Imaging (MRI), Ultrasound scan, and many more. X-rays are ionizing radiation and cannot be used for frequent examinations, whereas MRI is non-ionizing, but it is costly and time-consuming. Ultrasound scan is frequently used in scanning and is noninvasive but suffers from the problem of low image quality, which can lead to incorrect diagnoses. The efficiency of these methods depends on how invasive, fast, and accurate the imaging method is. Recently, a new method called Photoacoustic Tomography (PAT) is gaining attention due to its ability to produce images with high resolution and high contrast in long penetration depths. A system matrix could be developed from the pseudospectral matrix by evaluating it on different time samples for different sensor locations. Compressive Sensing (CS) algorithms can thus be developed using the system matrix obtained, and their performance could be evaluated. CS is based on how sparse the reconstruction could be. This is mainly based on the regularizer used along with the prior information. In this paper, we propose split Bregman formulation of isotropic and anisotropic total variation with l_1 and l_2 regularization for efficient PAT image reconstruction. The proposed methods have better reconstruction efficiency in terms of computation time and image quality while maintaining the sparsity. When evaluating the various TV formulations for PAT image reconstruction, it is observed that anisotropic TV-l_2 is the most efficient one, generating superior image quality and accomplishing the reconstruction in less than 1 second, enabling quick medical imaging and early diagnosis.**

***Index Terms*—Total variation, Photoacoustic Tomography, Compressive Sensing, Split Bregman, Cancer Detection**

I. Introduction

Photoacoustic tomographic (PAT) imaging is a non-invasive biomedical imaging technique based on the photoacoustic effect utilized to obtain high-quality images at rapid speeds [1]. It is a significant technique for diagnosing morphological, physiological, and biochemical anomalies in human systems. In recent years, PAT imaging has made it possible for several intriguing imaging applications, such as the detection of hemoglobin, rheumatoid arthritis, functional brain imaging, oxygen saturation detection, ocular imaging, small animal imaging, and pre-clinical cancer diagnostics [2], [3].

In comparison to other functional imaging methods, photoacoustic imaging is exceptional in that it can access deep tissue structures and generate images with higher resolution [4]

By finding the linear inverse, an image can be extracted from a linear system. The least-squares (LS) or regularized LS solutions can thus be used as a general method to approximately solve a linear inverse. The solution can be rendered sparse if l_1 regularization is used instead of l_2 regularization. Sparsity is crucial since it enables quick computation and dimensionality reduction. Also, regularization avoids the problem from being ill-posed and constrains it to have a unique solution.

The growth of compressive sensing (CS) theory has drawn a lot of attention to l_1 norm regularization. A new paradigm in image processing called CS allows for the reconstruction of images with fewer samples [5]. Both data compression and sparse recovery have made extensive use of it. The benefits of adopting CS include reduced memory storage, a higher data transfer rate, a decrease in power consumption, and a lower necessity for sensory equipment. Therefore, CS might be used with PAT imaging to provide a high-resolution deep tissue imaging system with reduced computational effort

In this paper, initially, anisotropic Total Variation (TV) and isotropic TV for both l_1 and l_2 regularization are simulated and compared with some existing CS algorithms for PAT image reconstruction in terms of image quality and computation time. TV algorithms has been widely used for denoising and deblurring applications [6], [7], [8]. An analysis of weighted difference regularization of TV model, and comparison of difference of convex algorithms and Bregman iteration for image denoising and deblurring is investigated in [9].

The paper is arranged as follows. An overview of CS algorithms is provided in Section II. Section III describes the details of the proposed TV algorithms. In Section IV, results are discussed and a comparison of the proposed algorithms with some existing CS algorithms is done. The paper is concluded in Section V which also outlines future directions for CS reconstruction research.

II. Compressive Sensing

In PAT, the desired part of the tissue is heated using laser pulses and the sound waves that propagate are captured using a sensor [10]. The raw data (sensor measured data) is then used for image reconstruction. Accurate model-based methods can be utilized to efficiently reconstruct an image from the sensor measurements using the pseudospectral method. It is suggested to produce the same results as that of the k-Wave toolbox in MATLAB [11]. A system matrix could be developed from the pseudospectral matrix by evaluating it on different time samples for different sensor locations, to obtain the sensor data as

$$\mathbf{y} = \mathbf{M}\mathbf{x}, \tag{1}$$

where $\mathbf{y} \in \mathbb{R}^{N_s N_t \times 1}$ is the measurement vector obtained, $\mathbf{M} \in \mathbb{R}^{N_s N_t \times N_{in}^2}$ is the system matrix and $\mathbf{x} \in \mathbb{R}^{N_{in}^2 \times 1}$ is the image to be reconstructed (in vectorized form); N_s, N_t and N_{in}^2 are the number of sensors, number of time samples and the number of imaging grid points respectively [12]. CS algorithms can thus be developed using the system matrix obtained, and their performance could be evaluated. CS allows to reconstruct an image from fewer samples and this sparsity is enforced by using a regularization parameter with prior info. In this section, different CS algorithms starting from Least-Squares (LS) are discussed with l_1, l_2, and Total Variation regularized LS problems. Some commonly employed CS algorithms are listed as follows.

1) l_2 regularized LS: An l_2 regularized LS problem also known as Tikhonov regularization [13], [14], is formulated as

$$\mathbf{x}^* = \min_{\mathbf{x}} \|\mathbf{y} - \mathbf{M}\mathbf{x}\|_2^2 + \lambda \|\mathbf{x}\|_2^2, \tag{2}$$

where $\lambda > 0$ is the regularization parameter. This type of regularization can preserve edges when compared to the LS without regularization but still suffers from poor reconstruction due to error distribution [15].

2) Smoothed l_0 norm (SL0): The most sparse regularization that could be applied is l_0 norm regularization. As l_0 norm is NP-hard, a smoothed approximation is applied for its effecient implementation [16]. Generally, l_p norms for $0 \leq p < 1$, are non convex and non-differntiable, but could be solved effeciently when approximations or relaxations are used [17], [18], [19]. This is formulated as

$$\mathbf{x}^* = \min_{\mathbf{x}} \|\mathbf{y} - \mathbf{M}\mathbf{x}\|_2 + \lambda \|\mathbf{x}\|_p. \tag{3}$$

3) $l_1 - l_2$ minimization: It can be formulated as

$$\mathbf{x}^* = \min_{\mathbf{x}} (\|\mathbf{x}\|_1 - \|\mathbf{x}\|_2) \text{ s.t } \mathbf{M}\mathbf{x} = \mathbf{y}. \tag{4}$$

Two existing approaches that can solve a $l_1 - l_2$ minimization are Difference of Convex Analysis (DCA) [20], and Forward-Backward Splitting (FBS) [21], [22]. Both of these techniques work well for reconstructing a sparsity-preserving image, but they both compromise on image quality [21].

4) Basis Pursuit (BP): BP is a well known formulation which is both sparsity preserving and error tolerant [23], formulated as

$$\mathbf{x}^* = \arg\min_{\mathbf{x}} \|\mathbf{x}\|_1 \text{ s.t } \mathbf{M}\mathbf{x} = \mathbf{y}. \tag{5}$$

The existing tools to solve a BP problem, namely CVX [24] and l_1-MAGIC [5] suffers from being computationally expensive [25]. In this paper, BP using ADMM formulation is considered, which is sought to be the efficient method of formulating the BP problem.

5) Total variation (TV) regularized LS: Another regularization that is commonly being used in medical imaging is TV, proposed by Rudin, et.al [26], is capable of preserving edges. It is formulated as

$$\mathbf{x}_{TV} = \min_{\mathbf{x}} \|\mathbf{D}\mathbf{x}\|_p \text{ s.t. } \mathbf{M}\mathbf{x} = \mathbf{y}, \tag{6}$$

where $\mathbf{D}$ is a difference matrix defined as:

$$\mathbf{D} = \begin{bmatrix} -1 & 1 & & & \\ & -1 & 1 & & \\ & & \cdots & \cdots & \\ & & & -1 & 1 \end{bmatrix}.$$

When $p = 1$, (6) is referred to as an anisotropic TV problem and as isotropic-TV when $p = 2$. Different applications of TV regularized LS problems have been discussed in [27], [28] and [29] for filtering, de-noising and restoring images.

Among the above-mentioned algorithms, BP and TV have been proved to be efficient. But, BP takes more computation time to converge to a solution when compared to TV, when different formulations of the two are considered.

III. Total Variation

In this section, isotropic and anisotropic TV formulation using split Bregman method is proposed and derived. It is seen to produce better results than the other algorithms. Instead of reducing the non-differentiable convex function, as in (6), Bregman iteration (BI) allows one to find the extremum of a convex function by minimizing the Bregman distance. If a linearization is not applied, BI becomes computationally expensive. In contrast to BI, Split Bregman (SB) divides the original problem into equivalent subproblems and solves them through an iterative process [30], [31]. Therefore, it is possible to precisely minimize the subproblems, which enables effective computation. Additionally, SB employs variable splitting and can be applied with augmented Lagrangian to reconstruct high contrast images with fewer staircase effects. Here we focus on isotropic and anisotropic TV formulation based on split Bregman, and solve the subproblems iteratively for all formulations and their performances are finally compared (as in Section IV). Initially, we define the TV norm as primarily the l_1 norm of derivatives, and a TV regularized LS problem is formulated as in (6). It can be transformed to an unconstrained equation as

$$\mathbf{x}^* = \arg\min_{\mathbf{x}} \|\mathbf{D}\mathbf{x}\|_p + \frac{\beta}{2}\|\mathbf{M}\mathbf{x} - \mathbf{y}\|_2^2. \tag{7}$$

A regularization term $\frac{\alpha}{2}\|x\|_q$, where $q = 1$ corresponds to l_1 regularization and $q = 2$ corresponds to l_2 regularization, is added to (7) as:

$$\mathbf{x}^* = \arg\min_{\mathbf{x}} \|\mathbf{D}\mathbf{x}\|_p + \frac{\beta}{2}\|\mathbf{M}\mathbf{x} - \mathbf{y}\|_2^2 + \frac{\alpha}{2}\|\mathbf{x}\|_q. \tag{8}$$

Transforming (8) into a constrained problem by introducing a new variable $\mathbf{d} = \mathbf{Dx}$, to enable decoupling as:

$$(\mathbf{x}^*, \mathbf{d}^*) = \arg\min_{\mathbf{x},\mathbf{d}} \|\mathbf{d}\|_p + \frac{\beta}{2}\|\mathbf{Mx} - \mathbf{y}\|_2^2 + \frac{\alpha}{2}\|\mathbf{x}\|_q \quad \text{s.t. } \mathbf{d} = \mathbf{Dx}. \quad (9)$$

Hence, (9) can be transformed to an unconstrained problem as:

$$(\mathbf{x}^*, \mathbf{d}^*) = \arg\min_{\mathbf{x},\mathbf{d}} \|\mathbf{d}\|_p + \frac{\beta}{2}\|\mathbf{Mx} - \mathbf{y}\|_2^2 + \frac{\gamma}{2}\|\mathbf{d} - \mathbf{Dx}\|_2^2 + \frac{\alpha}{2}\|\mathbf{x}\|_q. \quad (10)$$

Now, introducing the Bregman parameter $\mathbf{b}$ to (10) as

$$(\mathbf{x}^{k+1}, \mathbf{d}^{k+1}) = \arg\min_{\mathbf{x},\mathbf{d}} \|\mathbf{d}\|_p + \frac{\beta}{2}\|\mathbf{Mx} - \mathbf{y}_2^2 + \frac{\alpha}{2}\|\mathbf{x}\|_q + \frac{\gamma}{2}\|\mathbf{d} - \mathbf{Dx} - \mathbf{b}\|_2^2, \quad (11)$$

and $\mathbf{b}$ is updated as:

$$\mathbf{b}^{k+1} = \mathbf{b}^k + \mathbf{d}^k - \mathbf{Dx}^{k+1}. \quad (12)$$

From (11), the different cases of TV formulations can be considered as follows. The update of Bregman parameter $\mathbf{b}$, has the same equation for all cases. The difference is with the updates of $\mathbf{x}$ and $\mathbf{d}$ as explained below.

Case 1: Isotropic TV-$l_2; p = 2, q = 2$

$$\mathbf{x}^{k+1} \leftarrow (\alpha\mathbf{I} + \beta\mathbf{M}^T\mathbf{M} + \gamma\mathbf{D}^T\mathbf{D})^{-1}(\beta\mathbf{M}^T\mathbf{y} + \gamma\mathbf{D}^T(\mathbf{d}^k - \mathbf{b}^k)) \quad (13)$$

$$\mathbf{d}^{k+1} \leftarrow \mathbf{Dx}^{k+1} + \mathbf{b}^k. \quad (14)$$

Case 2: Isotropic TV-$l_1; p = 2, q = 1$

$$\mathbf{x}^{k+1} \leftarrow \text{Shrink}((\beta\mathbf{M}^T\mathbf{M} + \gamma\mathbf{D}^T\mathbf{D})^{-1}(\beta\mathbf{M}^T\mathbf{y} + \gamma\mathbf{D}^T(\mathbf{d}^k - \mathbf{b}^k)), \frac{1}{\alpha}) \quad (15)$$

$$\mathbf{d}^{k+1} \leftarrow \mathbf{Dx}^{k+1} + \mathbf{b}^k. \quad (16)$$

Case 3: Anisotropic TV-$l_2; p = 1, q = 2$

$$\mathbf{x}^{k+1} \leftarrow (\alpha\mathbf{I} + \beta\mathbf{M}^T\mathbf{M} + \gamma\mathbf{D}^T\mathbf{D})^{-1}(\beta\mathbf{M}^T\mathbf{y} + \gamma\mathbf{D}^T(\mathbf{d}^k - \mathbf{b}^k)) \quad (17)$$

$$\mathbf{d}^{k+1} \leftarrow \text{Shrink}(\mathbf{Dx}^{k+1} + \mathbf{b}^k, \frac{2}{\gamma}) \quad (18)$$

Case 4: Anisotropic TV-$l_1; p = 1, q = 1$

$$\mathbf{x}^{k+1} \leftarrow \text{Shrink}((\beta\mathbf{M}^T\mathbf{M} + \gamma\mathbf{D}^T\mathbf{D})^{-1}(\beta\mathbf{M}^T\mathbf{y} + \gamma\mathbf{D}^T(\mathbf{d}^k - \mathbf{b}^k)), \frac{1}{\alpha}) \quad (19)$$

$$\mathbf{d}^{k+1} \leftarrow \text{Shrink}(\mathbf{Dx}^{k+1} + \mathbf{b}^k, \frac{2}{\gamma}) \quad (20)$$

$\text{Shrink}(\cdot)$ in the above equations is the soft thresholding function defined as:

$$\text{Shrink}(\theta, \eta) = \begin{cases} (|\theta| - \eta)\,\text{sgn}(\theta) & \text{if } |\theta| > \eta \\ 0 & \text{otherwise} \end{cases}. \quad (21)$$

Altogether, the SB-TV algorithms can be summarized as in Algorithm 1.

Algorithm 1 Split Bregman Iteration for TV minimization

Require: $\alpha, \beta, \gamma > 0$, tol, maxit
Initialize: $k = 0$, NMSE = ∞, $\mathbf{x}^k = \mathbf{0}$, $\mathbf{d}^k = \mathbf{b}^k = \mathbf{0}$
while $\text{NMSE}^k > \text{tol} \vee k < \text{maxit}$ **do**

$$\mathbf{x}^{k+1}, \mathbf{d}^{k+1} \leftarrow \begin{cases} (13), (14); & \text{for Isotropic TV-}l_2 \\ (15), (16); & \text{for Isotropic TV-}l_1 \\ (17), (18); & \text{for Anisotropic TV-}l_2 \\ (19), (20); & \text{for Anisotropic TV-}l_1 \end{cases}$$

$\mathbf{b}^{k+1} \leftarrow \mathbf{b}^k + \mathbf{d}^{k+1} - \mathbf{Dx}^{k+1}$

$\text{NMSE}^{k+1} \leftarrow \frac{\|\mathbf{x}^{k+1} - \mathbf{x}^k\|_2^2}{\|\mathbf{x}^{k+1}\|_2^2}$

$k \leftarrow k + 1$
end while

IV. Results

In this section, the proposed Anisotropic SBTV-l_1, Anisotropic SBTV-l_2, Isotropic SBTV-l_1, and Isotropic SBTV-l_2 are compared with LS, regularized LS, BP, LASSO, iterative sparsification projection (ISP) of l_0 norm using alternating direction method of multipliers (SL0-ADMM), DCA and FBS (for $l_1 - l_2$) formulations. The following measures are used to evaluate the performance.

1) Structural similarity index (SSIM) [32] : Its value ranges from -1 to $+1$ and is used to evaluate image quality. Its value is around $+1$ when the reconstructed image resembles the original image.
2) Normalized mean-squared error (NMSE): It is the normalized mean-squared error between the reconstructed image and the original image defined as:
$$\text{NMSE} = \frac{\|\hat{\mathbf{x}} - \mathbf{x}\|_2^2}{\|\mathbf{x}\|_2^2} \quad (22)$$
where $\hat{\mathbf{x}}$ is the estimated image (or the reconstructed image from measurements).
3) Gini index (GI): GI is used to measure sparsity. The higher the value of GI, the more sparse the image is. Its value ranges from 0 to 1. In the simulations below, the original image has a GI of 0.5785.
4) Computational complexity: When calculating the computational complexity, the runtime is taken into account.
5) Iterations: The algorithm's convergence is assessed by the number of iterations required. Otherwise specified, the simulation's maximum iteration count is typically set at 100.

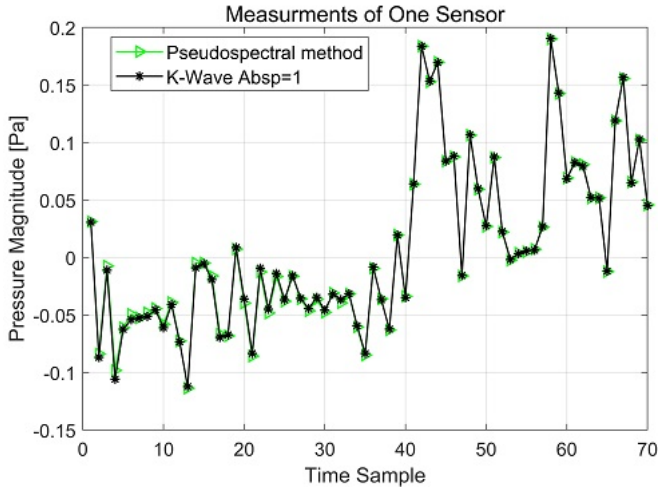

Fig. 1: Comparison of sensor data from K-wave and from pseudo-spectral matrix for one particular sensor, for 75 samples with 0.1mm spacing.

For computing the SSIM and GI, the built-in functions in MATLAB were used. The maximum frequency is calculated as $F_m = \frac{c}{2\Delta}$, where Δ is the grid spacing, and $c = 1500$m/s is the speed of sound. The sampling frequency is $F_s = 2F_m$, and the acquisition time is fixed at $t_q = 5$ μseconds. The total number of samples is thus found as $N_t = t_q \times F_s$ samples. In the setup, a grid spacing of $\Delta = 0.1$mm is considered. A total number of sensors $N_s = 71$ is used in the simulations distributed in a square grid around the object. The processor used in the simulation is Intel®Core™ i7-8565U 1.8GHz with MATLAB®. Initially, a pseudospectral method is used to develop the system matrix, which allows the formulation of different CS algorithms. The measurements obtained from the pseudospectral method, for one sensor, are then compared with that obtained from the k-wave [11] and are found to be approximately the same, as shown in Figure 1, with a mean square error of 3.54e-4. The sensor data obtained from the K-wave and the system matrix from the pseudospectral method are then utilized to reconstruct the image by employing the different CS algorithms.

Table. I shows the simulation results for different reconstruction algorithms. Figure 2 shows the original image and the reconstructed images for non-iterative algorithms (LS and Tikhonov regularized LS). They exhibit a closed-form solution and thus are not solved iteratively. In these, the noise and the error get distributed and produce a highly distorted image. Thus the non-iterative algorithms have the worst performance and are not suited for PAT image reconstruction [15].

Figure 3 shows the reconstructed images for l_1, $l_1 - l_2$ and SL0 iterative algorithms. The $l_1 - l_2$ formulations (DCA and FBS) tend to find a solution but are not suitable for a high contrast fast reconstruction. The l_1 minimization, using l_1-MAGIC has the best SSIM of all, but they are complex and computationally heavy (as they take very high time for computation) and are thus not suited.

(a) original image (b) 0.2994 (c) 0.0064

Fig. 2: (a) Original Image. Reconstructed images when (b) Tikhonov regularization and (c) LS are used and the corresponding SSIM.

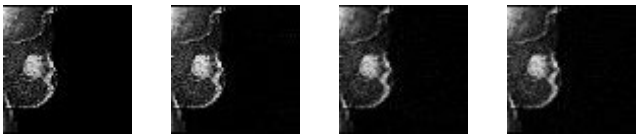

(a) 0.9518 (b) 0.7679 (c) 0.4595 (d) 0.6094

Fig. 3: Reconstructed images when (a) BP-ADMM (b) DCA $l_1 - l_2$ (c) FBS $l_1 - l_2$ and (d) SL0- norm algorithms are used and the corresponding SSIM.

It is observed that the proposed SBTV formulations exhibit outstanding performance when compared to the existing algorithms. The best formulation proposed is anisotropic-TV as it produces a more high-quality image than the isotropic formulations as in Figure 4. Moreover, the isotropic TV-l_2, exhibits a closed-form solution for all the three updates and is thus resembling an LS solution though it is iteratively solved and hence does not yield a suitable image. Furthermore, the proposed algorithms have computation time in the range of 1 second, which is most suited for a fast reconstruction algorithm.

TABLE I: Performance analysis for PAT image reconstruction for the case of 71 sensors.

Method	SSIM	NMSE	GI	iter	time [sec]
Anisotropic SBTV-l_1	0.9880	9.0e-7	0.5772	27	0.960
Anisotropic SBTV-l_2	0.9841	9.0e-7	0.5745	28	0.997
Isotropic SBTV-l_1	0.9771	1.5e-6	0.5758	51	1.798
Isotropic SBTV-l_2	0.7638	9.3e-7	0.5710	29	0.920
BP-ADMM	0.9518	6.7e-3	0.5822	48	13.90
DCA $l_1 - l_2$	0.7679	1.8e-3	0.5751	19	12.70
FBS $l_1 - l_2$	0.4595	4.2e-2	0.5890	292	159.2
SL0-ADMM	0.6094	3.6e-2	0.7716	51	3.945
l_1-MAGIC LASSO	1.0000	5.0e-4	0.7714	28	150.0
l_1-MAGIC BP	1.0000	1.3e-7	0.7714	8	1941
RLS(0.01)	0.2994	3.3e-1	0.7103	NA	13.69
LS	0.0064	9.0e+3	0.9995	NA	13.33

V. CONCLUSION

In this paper, a performance analysis of different formulations of TV algorithms, for PAT image reconstruction algorithms is carried out. The key feature of our algorithms is the use of Bregman splitting for decoupling the l_1 and l_2 norms to make convergence faster. Furthermore, SBTV exhibited

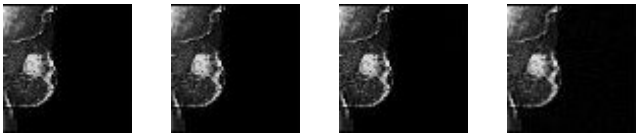

(a) 0.9880 (b) 0.9841 (c) 0.9771 (d) 0.7368

Fig. 4: Reconstructed images when (a)Anisotropic SBTV-l_1 (b)Anisotropic SBTV-l_2 (c)Isotropic SBTV-l_1 (d)Isotropic SBTV-l_2 are used and the corresponding SSIM.

a great reduction in the runtime and allow a way quicker reconstruction (< 1 seconds). The simulation results showed it had enhanced performance over other algorithms. For their runtime complexity and image reconstruction quality, SBTV algorithms demonstrate to have promising outcomes for PAT image reconstruction. We believe that the presented approaches can be expanded for more image processing applications and show promising application potential in the area of PAT medical imaging. The research's proposed next step is to construct the iterations utilizing layers of neural networks, which could increase the efficacy even more.

REFERENCES

[1] N. Meimani, N. Abani, J. Gelovani, and M. R. Avanaki, "A numerical analysis of a semi-dry coupling configuration in photoacoustic computed tomography for infant brain imaging," *Photoacoustics*, vol. 7, pp. 27–35, 2017.

[2] J. Shah, S. Park, S. R. Aglyamov, T. Larson, L. Ma, K. V. Sokolov, K. P. Johnston, T. E. Milner, and S. Y. Emelianov, "Photoacoustic imaging and temperature measurement for photothermal cancer therapy," *Journal of biomedical optics*, vol. 13, no. 3, p. 034024, 2008.

[3] H. Lan, T. Duan, D. Jiang, H. Zhong, M. Zhou, and F. Gao, "Dual-contrast nonlinear photoacoustic sensing and imaging based on single high-repetition-rate pulsed laser," *IEEE Sensors Journal*, vol. 19, no. 14, pp. 5559–5565, 2019.

[4] J. L. Su, B. Wang, K. E. Wilson, C. L. Bayer, Y.-S. Chen, S. Kim, K. A. Homan, and S. Y. Emelianov, "Advances in clinical and biomedical applications of photoacoustic imaging," *Expert opinion on medical diagnostics*, vol. 4, no. 6, pp. 497–510, 2010.

[5] E. Candes and J. Romberg, "l1-magic: Recovery of sparse signals via convex programming," *URL: www. acm. caltech. edu/l1magic/downloads/l1magic. pdf*, vol. 4, p. 14, 2005.

[6] G. Ma, Z. Yan, Z. Li, and Z. Zhao, "Efficient iterative regularization method for total variation-based image restoration," *Electronics*, vol. 11, no. 2, p. 258, 2022.

[7] H. Birkholz, "A unifying approach to isotropic and anisotropic total variation denoising models," *Journal of computational and applied mathematics*, vol. 235, no. 8, pp. 2502–2514, 2011.

[8] Y. Shi and Q. Chang, "Efficient algorithm for isotropic and anisotropic total variation deblurring and denoising," *Journal of Applied Mathematics*, vol. 2013, 2013.

[9] Y. Lou, T. Zeng, S. Osher, and J. Xin, "A weighted difference of anisotropic and isotropic total variation model for image processing," *SIAM Journal on Imaging Sciences*, vol. 8, no. 3, pp. 1798–1823, 2015.

[10] P. Kuchment and L. Kunyansky, "Mathematics of thermoacoustic tomography," *European Journal of Applied Mathematics*, vol. 19, no. 2, pp. 191–224, 2008.

[11] B. E. Treeby and B. T. Cox, "k-wave: Matlab toolbox for the simulation and reconstruction of photoacoustic wave fields," *Journal of biomedical optics*, vol. 15, no. 2, p. 021314, 2010.

[12] J. Provost and F. Lesage, "The application of compressed sensing for photo-acoustic tomography," *IEEE Transactions on Medical Imaging*, vol. 28, no. 4, pp. 585–594, 2009.

[13] M. T. Heath, "Numerical methods for large sparse linear least squares problems," *SIAM Journal on Scientific and Statistical Computing*, vol. 5, no. 3, pp. 497–513, 1984.

[14] I. Selesnick, "Least squares with examples in signal processing," *Connexions*, vol. 4, 2013.

[15] M. J. John and I. Barhumi, "Fast and efficient pat image reconstruction algorithms: A comparative performance analysis," *Signal Processing*, vol. 201, p. 108691, 2022.

[16] L. Zheng, A. Maleki, H. Weng, X. Wang, and T. Long, "Does lp - minimization outperform l1 - minimization?" *IEEE Transactions on Information Theory*, vol. 63, no. 11, pp. 6896–6935, 2017.

[17] J. Li, Z. Wu, H. Feng, Q. Wang, and Y. Liu, "Greedy orthogonal matching pursuit algorithm for sparse signal recovery in compressive sensing," in *2014 IEEE International Instrumentation and Measurement Technology Conference (I2MTC) Proceedings*. IEEE, 2014, pp. 1355–1358.

[18] M. Sadeghi and M. Babaie-Zadeh, "Iterative sparsification-projection: Fast and robust sparse signal approximation," *IEEE Transactions on Signal Processing*, vol. 64, no. 21, pp. 5536–5548, 2016.

[19] X.-F. Fang, J.-S. Zhang, and Y.-Q. Li, "Sparse signal reconstruction based on multiparameter approximation function with smoothed norm," *Mathematical Problems in Engineering*, vol. 2014, 2014.

[20] Y. Lou, P. Yin, Q. He, and J. Xin, "Computing sparse representation in a highly coherent dictionary based on difference of l1 and l2," *Journal of Scientific Computing*, vol. 64, no. 1, pp. 178–196, 2015.

[21] Y. Lou and M. Yan, "Fast l1–l2 minimization via a proximal operator," *Journal of Scientific Computing*, vol. 74, no. 2, pp. 767–785, 2018.

[22] T. Goldstein, C. Studer, and R. Baraniuk, "A field guide to forward-backward splitting with a fasta implementation," *arXiv preprint arXiv:1411.3406*, 2014.

[23] S. Chen and D. Donoho, "Basis pursuit," in *Proceedings of 1994 28th Asilomar Conference on Signals, Systems and Computers*, vol. 1, 1994, pp. 41–44 vol.1.

[24] M. Grant and S. Boyd, "CVX: Matlab software for disciplined convex programming, version 2.1," http://cvxr.com/cvx, Mar. 2014.

[25] K. Usman, H. Gunawan, and A. B. Suksmono, "Compressive sensing reconstruction algorithm using l1-norm minimization via l2-norm minimization." *International Journal on Electrical Engineering & Informatics*, vol. 10, no. 1, 2018.

[26] L. I. Rudin, S. Osher, and E. Fatemi, "Nonlinear total variation based noise removal algorithms," *Physica D: nonlinear phenomena*, vol. 60, no. 1-4, pp. 259–268, 1992.

[27] A. Chambolle, "An algorithm for total variation minimization and applications," *Journal of Mathematical imaging and vision*, vol. 20, no. 1, pp. 89–97, 2004.

[28] A. Beck and M. Teboulle, "A fast iterative shrinkage-thresholding algorithm for linear inverse problems," *SIAM journal on imaging sciences*, vol. 2, no. 1, pp. 183–202, 2009.

[29] M. Zhu, S. J. Wright, and T. F. Chan, "Duality-based algorithms for total-variation-regularized image restoration," *Computational Optimization and Applications*, vol. 47, no. 3, pp. 377–400, 2010.

[30] L. M. Bregman, "The relaxation method of finding the common point of convex sets and its application to the solution of problems in convex programming," *USSR computational mathematics and mathematical physics*, vol. 7, no. 3, pp. 200–217, 1967.

[31] S. Osher, M. Burger, D. Goldfarb, J. Xu, and W. Yin, "An iterative regularization method for total variation-based image restoration," *Multiscale Modeling & Simulation*, vol. 4, no. 2, pp. 460–489, 2005.

[32] V. Bruni and D. Vitulano, "An entropy based approach for ssim speed up," *Signal Processing*, vol. 135, pp. 198–209, 2017.